$$BW = \lambda_w \cdot [\sin\theta_N - \sin\theta_1]/\sin\theta_w \quad (2)$$

The equalisation region, W_E, is

$$W_E = BW - 2\cdot\delta\lambda = \lambda_w\cdot[\sin\theta_N - \sin\theta_1]/\sin\theta_w - 2\cdot\delta\lambda \quad (3)$$

where $\delta\lambda$ is the wavelength selectivity obtained from eqn. 1, and the centre-wavelength of the filter can be expressed as $\lambda_C = (\lambda_1 + \lambda_N)/2$.

Accordingly, the 3dB bandwidth is determned by the angular range $\Delta\theta$, which could be varied by f and d, i.e. the small focal length and larger width provide larger BW and W_E. This results in a larger controlled wavelength region.

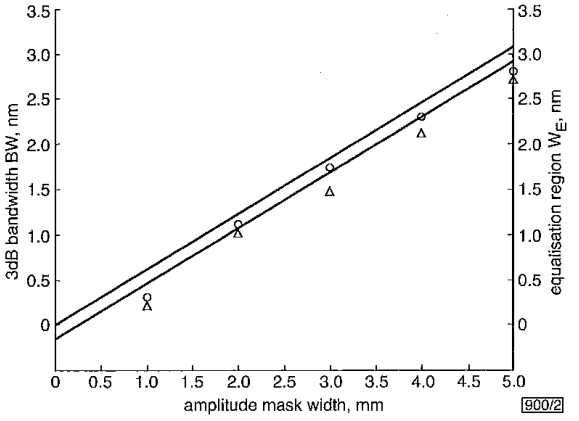

Fig. 2 *Experimental results of 3dB bandwidth and equalisation region against variations in amplitude mask width*

——— theoretical 3dB bandwidth
○ experimental 3dB bandwidth
– – – – theoretical equalisation region
△ experimental equalisation region

Experiment: The requred hologram is recorded by a He-Ne laser with a half-crossing angle of 45°. The light intensities of the recording beams are 8.9 and 9.25mW/cm^2. Both beams were ordinarily polarised with respect to the optical axis of the crystal. To avoid subsequent erasure owing to readout, the recorded hologram is thermally fixed at 180°C.

Reading of the hologram is carried out with a tunable laser source (660–680nm wavelength, 0.01nm resolution). It is expanded and collimated by a lens set, and passed through the amplitude mask and converging lens. We have used five masks between 1 and 5mm, with spacing of 1mm, and the focal length of the converging lens is 400mm. To obtain the centre-wavelength of 670nm, the incident angle θC is 48.476°.

The diffraction intensities are measured for various wavelengths of the readout beam with respect to the five amplitude masks. Fig. 2 shows the experimental results obtained from the optical setup shown in Fig. 1*a*. In Fig. 2, the solid line and the circles represent theoretical and experimental values for the 3dB bandwidth BW, respectively. Theoretical and experimental equalisation of region W_E are shown in Fig. 2 by the dashed line and the triangles. The experimental results show that the 3dB bandwidth of the filter is linearly increased between 0.35 and 3.3nm as the width of the amplitude mask varies. These results are only obtained by control of the mask width, and demonstrate potential application as a novel dynamic passband filter. In addition, the equalisation region of the filter varies from 0.2 to 2.7nm, which is in good agreement with theoretically expected values obtained from eqn. 3, and this region will enable stable filtering in multichannel WDM systems.

The control parameters of these properties (BW, W_E) are the width of the amplitude mask (d), the focal length of the converging lens (f) and the wavelength selectivity ($\delta\lambda$) of the grating. Narrower masks and longer focal lengths will permit narrowband filtering. The larger variable mask and shorter focal length expand the control region of the 3dB bandwidth. The narrower wavelength selectivity, $\delta\lambda$, achieves the larger equalisation region, W_E, with the fixed 3dB bandwidth. Using the above relations, the filter properties could easily be adjusted, in contrast to the use of other methods. The centre-wavelength is 670.1nm, which coincides with the designed conditions and can be controlled by variation of θ_C.

Conclusions: Amplitude masks and converging wave in photorefractive holographic grating enable effective passband control with the centre-wavelength of 670nm. Bandwidth variation has been demonstrated from 0.35 to 3.3nm, and will be expanded by the use of other lenses or masks. Our investigation shows that the converging wave in holographic grating is a potentially useful method for dynamic selection among different wavelength channels at the receiver end of a dense WDM transmission system.

21 August 2000
Electronics Letters Online No: 20001443
DOI: 10.1049/el:20001443

Jun-Won An and Nam Kim (*Department of Computer & Communication Engineering, Chungbuk National University, San 48, Gaeshin-Dong, Cheongju-City, Chungbuk, 361-763, Korea*)

E-mail: jwahn@osp.chungbuk.ac.kr

Kwon-Yeon Lee (*Department of Electronics Engineering, Sunchon National University, 315, Maegok-Dong, Sunchon-City, Chonnam, Korea*)

References

1 HUBNER, J., ZAUNER, D., and KRISTENSEN, M.: 'Strong sampled Bragg grating for WDM applications', *IEEE Photonics Technol. Lett.*, 1998, **10**, (4), pp. 552–554

2 HERMANN, H., SCHAFER, K., and SCHMIDT, C.: 'Low loss tunable integrated acousto optical wavelength filter in $LiNbO_3$ with strong sidelobe suppression', *IEEE Photonics Technol. Lett.*, 1998, **10**, (1), pp. 120–122

3 BREER, S., VOGT, H., NEE, I., and BUSE, K.: 'Low crosstalk WDM by Bragg diffraction from thermally fixed reflection holograms in lithium niobate', *Electron. Lett.*, 1998, **34**, (25), pp. 2419–2421

4 ZHU, P., LIU, X., and XU, A.: 'Color holography using the angular selectivity of volume recording media', *Appl. Opt.*, 1995, **34**, (5), pp. 842–845

Extremely broadband InGaAsP/InP superluminescent diodes

Bing-Ruey Wu, Ching-Fuh Lin, Lih-Wen Laih and Tien-Tsorng Shih

Record broadband characteristics of superluminescent diodes (SLD) are reported. Using two 87Å $In_{0.53}Ga_{0.47}As$ quantum wells and three 60Å $In_{0.67}Ga_{0.33}As_{0.72}P_{0.28}$ quantum wells, the fabricated SLDs exhibit a very broad emission spectrum. The spectral width is nearly 300nm, covering the range from 1300 to 1585.5nm.

Broadband characteristics are attractive for optical fibre communication. Recent technology has made optical fibres exhibit extremely broad bandwidths, almost covering the range from 1.2–1.6μm with a loss of less than 1dB/km. Although Er-doped fibre amplifiers (EDFAs) and lasers can be conveniently used in optical communication systems, their bandwidth is no more than 80nm (C-band: 1530–1565nm; L-band: 1570–1610nm) [1]. Thus the abundant bandwidth is still not fully exploited. By contrast, superluminescent diodes (SLDs)/semiconductor optical amplifiers (SOAs) are also good candidates for optical fibre communication systems because they are of compact size, can be directly integrated with electronic components, and their wavelength can be engineered. However, each SOA usually has a bandwidth of less than 50nm. To cover the entire usable bandwidth of an optical fibre, many SLDs/SOAs having different spectral ranges are required. Therefore, if the bandwidth of SLDs/SOAs could be broadened, they will be even more attractive. Multiple quantum well (MQW) engineering is a convenient way that has been widely used to broaden the bandwidth of SOAs/SLDs [2]. However, the design is not straightforward because the carrier distribution within the MQW is not uniform [3]. By considering the nonuniform carrier distribution within MQWs, we demonstrate that the spectral bandwidth of SLDs/SOAs can be significantly broadened by using properly designed nonidentical MQWs grown on InP substrate.

To achieve the broadband characteristics, a sequence of nonidentical MQWs are designed. The layer structure is shown in

Fig. 1. The two 87Å $In_{0.53}Ga_{0.47}As$ quantum wells, designed for a transition energy corresponding to 1.55μm, are grown near the *n*-cladding layer, while the three 60Å $In_{0.67}Ga_{0.33}As_{0.72}P_{0.28}$ quantum wells, designed for a transition energy corresponding to 1.3μm, are grown near the *p*-cladding layer. $In_{0.86}Ga_{0.14}As_{0.3}P_{0.7}$ barriers of 150Å width are used to separate the QWs. The separate confinement heterostructure (SCH) layer is 1200Å thick.

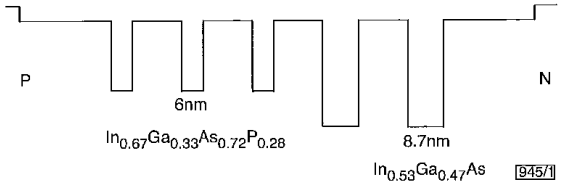

Fig. 1 *Quantum-well structure of designed nonidentical MQWs*

Barrier: 15nm, $In_{0.86}Ga_{0.14}As_{0.3}P_{0.7}$
SCH region: 120nm, $In_{0.86}Ga_{0.14}As_{0.3}P_{0.7}$

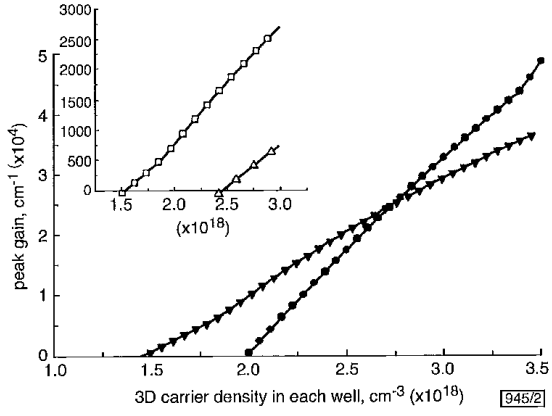

Fig. 2 *Calculated peak gain against carrier density in each well of $In_{0.53}Ga_{0.47}As$ double QW and $In_{0.67}Ga_{0.33}As_{0.72}P_{0.28}$ triple QW*

● 1.3μm 6nm TQW
▼ 1.55μm 8.7nm DQW
Inset: Peak gain against carrier density relation of $In_{0.53}G_{0.47}As$ and $In_{0.67}Ga_{0.33}As_{0.72}P_{0.28}$ single QW
□ 1.55μm 6nm SQW
△ 1.33μm 8.7nm SQW

Fig. 2 shows the theoretical calculation of peak gain against carrier density of the $In_{0.53}Ga_{0.47}As$ double QWs and $In_{0.67}Ga_{0.33}As_{0.72}P_{0.28}$ triple QWs. The gain spectrum is calculated using the Luttinger-Kohn method [4, 5], and the peak gain is extracted from the calculated gain profile. The inset of Fig. 2 shows the peak gain against carrier density relation of an $In_{0.53}Ga_{0.47}As$ and $In_{0.67}Ga_{0.33}As_{0.72}P_{0.28}$ single QW. From the inset of Fig. 2, we can see that the peak gain of the $In_{0.53}Ga_{0.47}As$ single QW (1.55μm) is always higher than that of the $In_{0.67}Ga_{0.33}As_{0.72}P_{0.28}$ single QW (1.3μm). If the well number of each type is the same, the emission at 1.3μm will be negligible due to its significantly lower gain. Therefore, the number of the 1.3μm well is greater than that of the 1.55μm well. Fig. 2 demonstrates that the peak gain of $In_{0.67}Ga_{0.33}As_{0.72}P_{0.28}$ triple QWs surpasses the peak gain of $In_{0.53}Ga_{0.47}As$ double QWs for a 3D carrier density greater than a certain value in each well. Near this particular carrier density, the nonidentical MQW structure leads to a broadened spectrum as a result of the superposition of the gain spectrum of the two types of QW.

The designed nonidentical MQW structure was then grown on an InP substrate by MOCVD. Typical processing techniques were used to fabricate bent-waveguide SLDs [6]. With the bent-stripe structure, the reflection of light from the cleaved facet is reduced, thus minimising the influence of Fabry-Perot resonance [6]. The device is ~500μm long. The ridge waveguide was created by ECR-RIE and etching was stopped at ~100nm above the SCH layer. The fabrication is completed by *n*-contact metallisation and then the devices were cleaved apart. No facet coatings were applied to the devices.

The emission spectra of the fabricated devices at different current levels were measured and are shown in Fig. 3. Emission at a low injection current occurs at a wavelength corresponding to the $n = 1$ transition in the 87Å $In_{0.53}Ga_{0.47}As$ double QWs, which is 1.55μm. Note that the 87Å $In_{0.53}Ga_{0.47}As$ double QWs are near the *n*-cladding layer. Thus more carriers accumulate near the *n*-cladding layer, indicating that electrons are the dominant carrier. When the injection current increases, the emission spectrum is first broadened due to the simultaneous transitions of the $n = 1$ and $n = 2$ states in the 87Å $In_{0.53}Ga_{0.47}As$ double QWs. The emission contribution from the 60Å $In_{0.67}Ga_{0.33}As_{0.72}P_{0.28}$ triple QWs then becomes prominent when the injection current is increased to > 400mA. The contribution of the 60Å $In_{0.67}Ga_{0.33}As_{0.72}P_{0.28}$ triple QWs becomes even higher at increased injection levels. This can be explained by examining the curves shown in Fig. 2. Although the gain occurs at a lower carrier density for the 87Å $In_{0.53}Ga_{0.47}As$ double QWs than for the 60Å $In_{0.67}Ga_{0.33}As_{0.72}P_{0.28}$ triple QWs, the increasing rate of peak gain of the 60Å $In_{0.67}Ga_{0.33}As_{0.72}P_{0.28}$ triple QWs is larger than that of the 87Å $In_{0.53}Ga_{0.47}As$ double QWs. Therefore, the two kinds of MQW have almost equal gain at a particular injection level, resulting in an extremely broadband emission spectrum. The widest spectral width occurs at 600mA with a spectral width of 285.5nm, covering the 1300–1585.5nm range.

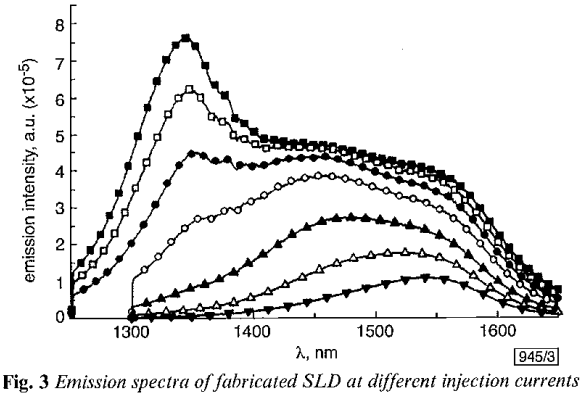

Fig. 3 *Emission spectra of fabricated SLD at different injection currents*

■ 1000mA
□ 800mA
◆ 600mA
◇ 400mA
▲ 200mA
△ 100mA
▼ 50mA
04291 bend amplifier, 500μm, straight side facet

When designing a broadband SOA using a nonidentical MQW structure, factors such as QW transition energy, number and sequence of the different QWs, the thickness of the SCH layer, the selection of the dominant carrier, the ability of the QW to trap the 2D carrier, the uniformity of the 2D carrier within the QWs, etc. must be taken into account. Using a properly designed nonidentical MQW structure, the fabrication of even more broadband SLDs should be possible.

Conclusion: We have demonstrated extremely broadband SLDs using two properly designed 87Å $In_{0.53}Ga_{0.47}As$ QWs and three 60Å $In_{0.67}Ga_{0.33}As_{0.72}P_{0.28}$ QWs. A spectral width covering a range from 1.3 to 1.55μm has been achieved. The spectral width could be as broad as 285.5nm.

Acknowledgment: This work is supported in part by the National Science Council, Taipei, Taiwan, Republic of China under contract No. NSC89-2215-E-002-016 and No. NSC89-2112-M-002-034.

23 August 2000
Electronics Letters Online No: 20001440
DOI: 10.1049/el:20001440

Bing-Ruey Wu and Ching-Fuh Lin (*Department of Electrical Engineering and Graduate Institute of Electro-Optical Engineering, National Taiwan University, Taipei, Taiwan, Republic of China*)

Lih-Wen Laih and Tien-Tsorng Shih (*Telecommunication Laboratory, Chunghua Telecom Co. Ltd., Yang-Mei, Taoyuan, Taiwan, Republic of China*)

References

1 STERN, T.E., and BALA, K.: 'Multiwavelength optical networks' (Addison-Wesley, MA, 1999), Chap. 4, pp. 193–199
2 SEMENOV, A.T., SHIDLOVSKI, V.R., and SAFIN, S.A.: 'Wide spectrum single quantum well superluminescent diodes at 0.8mm with bent optical waveguide', *Electron. Lett.*, 1993, **29**, pp. 854–857
3 LEE, B.L., LIN, C.F., LAI, J.W., and LIN, W.: 'Experimental evidence of nonuniform carrier distribution in multiple-quantum-well laser diodes', *Electron. Lett.*, 1998, **34**, pp. 1230–1231
4 AHN, D., and CHUANG, S.L.: 'Optical gain and gain suppression of quantum well lasers with valence band mixing', *IEEE J. Quantum Electron.*, 1990, **26**, pp. 13–24
5 CHUANG, S.L.: 'Physics of optoelectronic devices' (John Wiley & Sons, New York, 1995), Chap. 9
6 LIN, CHING-FUH, and CHAUR-SHIUANN, JUANG: 'Superluminescent diode with bent waveguide', *IEEE Photonics Technol. Lett.*, 1996, **8**, pp. 206–208

Germanium on silicon *pin* photodiodes for the near infrared

G. Masini, L. Colace, G. Assanto, H.C. Luan and L.C. Kimerling

Novel Ge on silicon *pin* photodetectors have been fabricated and characterised. The devices, designed by considering the defects at the Ge/Si interface, exhibit overall performances that are among the best available, with short-circuit responsivities as high as 0.4A/W at 1.3μm, dark currents below 20mA/cm² and response times shorter than 800ps.

The widespread demand for Internet services has caused an extensive and unprecedented diffusion of fibre optic communications. This demand has stimulated a great deal of research towards the fabrication of low-cost optical transceivers for the near infrared (NIR). In this framework, the integration of optoelectronic devices in silicon chips has been identified as one of the most viable approaches. Due to the compatibility of SiGe with Si CMOS technology, many researchers have focused on integrating SiGe photodiodes on Si [1, 2]. The challenge is the minimisation of the threading dislocations (TD) associated with the lattice mismatch between SiGe and Si. TDs seriously affect device performance and density typically increases with Ge concentration. Nevertheless, Ge-rich alloys are preferred for light detection owing to their higher absorption in the near infrared up to 1.6μm. Recently, we have demonstrated sensitive and fast NIR photodetectors fabricated by direct epitaxial growth of pure Ge on Si using a thin low-temperature Ge-buffer and cyclic thermal annealing [3]. These devices, based on unintentionally-doped Ge grown on *p*-type Si, exhibited a reduced short-circuit photoresponse owing to the low built-in electric field in the Ge film. In this Letter we investigate and demonstrate the integration of *pin* Ge photodiodes on Si to: (i) maximise the responsivity in short circuit; and (ii) minimise the dark current. Our *pin* structures consist of a thin heavily doped n^+-Ge (p^+) layer, an intrinsic Ge film (1μm) and a p^+-Si (n^+-Si) substrate. Employing heavily doped Si substrates permits simplification of both the Ge growth and the electrical connections to the diode.

To evaluate the best combination of substrate type and doping we modelled and simulated Ge/Si *pin* structures, taking into account the acceptor-like interface defect-states (in the forbidden gap) due to the lattice mismatch between Ge and Si [4]. Figs. 1*a* and *b* are calculated equilibrium band diagrams for Ge/Si heterojunctions on *p*- and *n*-Si substrates, respectively, for two resistivities: 1Ωcm and 0.01Ωcm. For the case with *p*-substrates, the electric field in the Ge film is monotonic; conversely, for *n*-substrates, two back connected diodes are formed owing to pinning of the acceptor-like states at the heterojunction. We expect free carriers generated in the Ge film (either by thermal or optical excitation) to flow more easily in diodes on *p*-Si than on *n*-Si substrates. This is confirmed by calculation results, shown in Fig. 2*a*, from which it is apparent that the dark current in Ge-on-(*p*-Si) diodes is almost independent from substrate doping. Devices on *n*-Si behave quite differently: at high substrate resistivities the triangular barrier at the Ge/Si interface hampers the extraction of the thermally-generated carriers, thus limiting the leakage current density; at lower resistivities barrier width and height at the Ge/Si interface are reduced, thus increasing the leakage current. Fig. 2*b* shows that the same limiting mechanism holds for photogenerated carriers. Therefore, Ge diodes on *p*-type substrate should be preferred owing to their higher responsivity and lower reverse current. In addition, since both dark current and responsivity do not depend on Si resistivity, we could choose the highest doping to get a better back-contact and a lower series resistance.

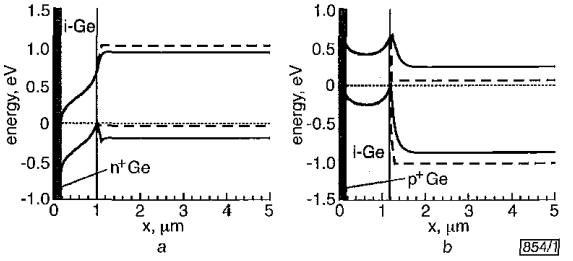

Fig. 1 *Calculated equilibrium band diagram of Ge/Si pin diodes*

a nip diode on *p*-Si
b pin diode on *n*-Si
– – – substrate resistivity = 1Ωcm
– – – – substrate resistivity = 0.01Ωcm

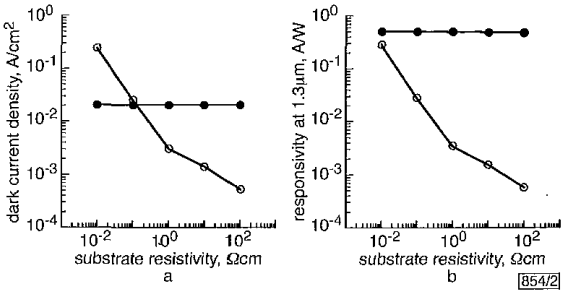

Fig. 2 *Calculated reverse dark current density and 1.3μm responsivity of Ge diodes on Si against substrate resistivity*

a Reverse dark current densities
b 1.3μm responsivities
○ *n*-Si substrate
● *p*-Si substrate

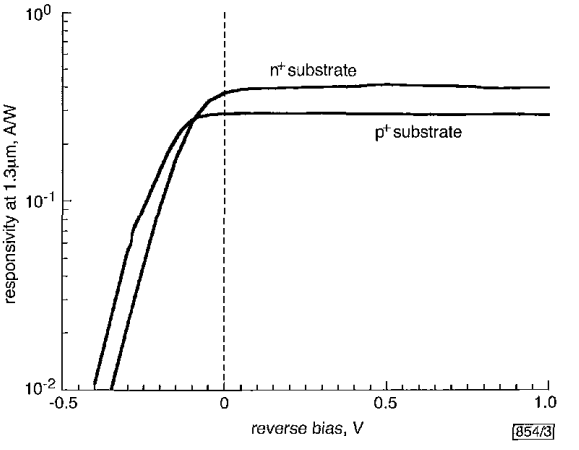

Fig. 3 *Measured 1.3μm responsivity of mesa pin Ge/Si diodes against reverse voltage*

Based on the above, we have fabricated Ge diodes on p^+ and n^+ silicon using the technique described elsewhere [3, 5]. p^+ and n^+ contacts were realised by ion implantation, mesa structures and ohmic metal contacts by standard photolithography and wet chemical etching. Measured dark reverse currents in diodes on p^+-Si are lower than in diodes on n^+-Si, as expected. In particular, Ge-on-p^+-Si diodes exhibit a reverse current density of 20mA/cm²